Acta Crystallographica Section D
Biological Crystallography
ISSN 0907-4449

Structure of pteridine reductase (PTR1) from *Leishmania tarentolae*

Haiyan Zhao,[a] Tom Bray,[a] Marc Ouellette,[b] Ming Zhao,[a] Rose Ann Ferre,[c] David Matthews,[c] John M. Whiteley[a] and Kottayil I. Varughese[a]*

[a]Department of Molecular and Experimental Medicine, The Scripps Research Institute, 10550 North Torrey Pines Road, La Jolla, CA 92037, USA, [b]Infectious Disease Research Centre, University of Laval, Quebec G1V 4G2, Canada, and [c]Pfizer Inc., 10770 Science Center Drive, San Diego, CA 92121, USA

Correspondence e-mail: kiv@scripps.edu

Received 21 April 2003
Accepted 12 June 2003

PDB Reference: *L. tarentolae* PTR1, 1p33, r1p33sf.

The protozoan parasites *Leishmania* utilize a pteridine-reducing enzyme, pteridine reductase (PTR1), to bypass antifolate inhibition. The crystal structure of PTR1 from *L. tarentolae* has been solved as a binary complex with NADPH at 2.8 Å resolution. The structure was solved by molecular-replacement techniques using the recently reported *L. major* PTR1 structure as a search model. Comparisons of the present structure with the *L. major* PTR1 allowed us to identify regions of flexibility in the molecule. PTR1 is a member of the growing family of short-chain dehydrogenases (SDR) which share the characteristic Tyr(Xaa)$_3$Lys motif in the vicinity of the active site. The functional enzyme is a tetramer and the crystallographic asymmetric unit contains a tetramer with 222 point-group symmetry.

1. Introduction

Leishmania are protozoan parasites that are responsible for considerable morbidity and mortality worldwide. These parasites are auxotrophs for both folates and pterins. They have developed complex transport and salvage systems to fulfil their folate and pterin requirements and some of these activities are potential new drug targets (reviewed in Nare, Luba *et al.*, 1997; Ouellette *et al.*, 2002). Our understanding of pteridine metabolism in these species is derived mostly from work on the mechanisms of resistance to the antifolate model drug methotrexate (MTX). One common mechanism involves the amplification of a gene coding for PTR1, a pteridine reductase. The main function of PTR1 is to salvage oxidized and 7,8-dihydropterins, including folic acid and dihydrofolate (Nare, Hardy *et al.*, 1997; Wang *et al.*, 1997). Antifolates have efficacy against several protozoan parasites, but they are not effective against *Leishmania*. This is because of the ability of PTR1 to act as an alternative pathway for providing reduced folates when the main target dihydrofolate reductase (DHFR) is blocked by antifolates. Thus, to be useful against *Leishmania*, antifolates would need to target both PTR1 and DHFR.

PTR1 belongs to the family of short-chain dehydrogenase/reductases (SDR), most of which are medium-sized proteins of about 250 amino acids. They have a dinucleotide-binding motif towards the N-terminus and a Tyr(Xaa)$_3$Lys signature motif toward the C-terminal portion of the protein. Our interest in SDR proteins led to the establishment of the structure of dihydropteridine reductase (DHPR), an enzyme that reduces the pterin quinonoid isomer but not oxidized pterins (Varughese *et al.*, 1992). We found that the Tyr(Xaa)$_3$Lys motif plays a crucial role in the reactions catalyzed by DHPR (Varughese *et al.*, 1994; Kiefer *et al.*, 1996). Additionally, we found that the molecule has a degree of

adaptability, as it resorts to alternate ways to restore the activity when mutations are carried out on the signature motif (Kiefer *et al.*, 1996). To enhance the understanding of the overall binding and catalytic mechanisms of SDRs, we have determined the structure of PTR1 derived from *L. tarentolae*, a parasite distantly related to *L. major*, for which a similar structure of PTR1 was recently reported (Gourley *et al.*, 2001). The reductive pathways for PTR1, DHFR and DHPR are shown in Fig. 1.

2. Experimental procedures

2.1. Expression and purification of PTR1

The *PTR1* gene was subcloned into a pET16b vector. Expression of the protein after IPTG induction followed by SDS gel analysis showed that PTR1 was the major soluble protein present in the cell supernatant (>50%). A large-scale purification by ammonium sulfate precipitation and DEAE-trisacryl chromatography showed that the protein contained in the middle fractions of the major eluted peak was essentially homogeneous (>99%) according to SDS gels and Coomassie Blue staining. Usually, the central peak fractions yielded 15–20 mg of pure protein per litre of culture. Molecular-weight measurements by Sephacryl S-100 filtration chromatography indicated a MW that was greater than 90 kDa, suggesting either a trimer or a tetramer. Further examination using 5–9% non-denaturing gel electrophoresis showed the protein to be tetrameric, with a molecular weight of ∼120 kDa. Similar results have been reported earlier for the PTR1 pMALc-2 fusion vector expression in *Escherichia coli* (Wang *et al.*, 1997). An experimental pI value of 5.1 was obtained for wild-type PTR1, which was consistent with the observation that this protein could be eluted at low salt concentrations (∼0.12 *M* NaCl) from DEAE-trisacryl resin.

2.2. Crystallization and data collection

The ternary complex of PTR1 with NADPH and methotrexate was prepared by mixing 20 µl of protein solution containing 20 mg ml^{-1} PTR1 in 20 m*M* Tris–HCl buffer pH 7.0 with 10 µl of a solution containing 4 m*M* NADPH and 4 m*M* methotrexate in 10 m*M* MOPS pH 7.0. The complex was incubated on ice for 1 h and used for crystallization. The ternary complex crystals were obtained at 287 K by the hanging-drop method. The reservoir solution contained 28% 1,4-butanediol, 12.5 m*M* cetyl trimethyl ammonium chloride (CTMC) and 100 m*M* HEPES at pH 7.0. The crystals grew in 5 d to maximum dimensions of 0.15 × 0.2 × 0.5 mm in space group $P2_12_12_1$, with unit-cell parameters a = 91.30, b = 96.10, c = 195.54 Å. The volume of the unit cell suggested there to be

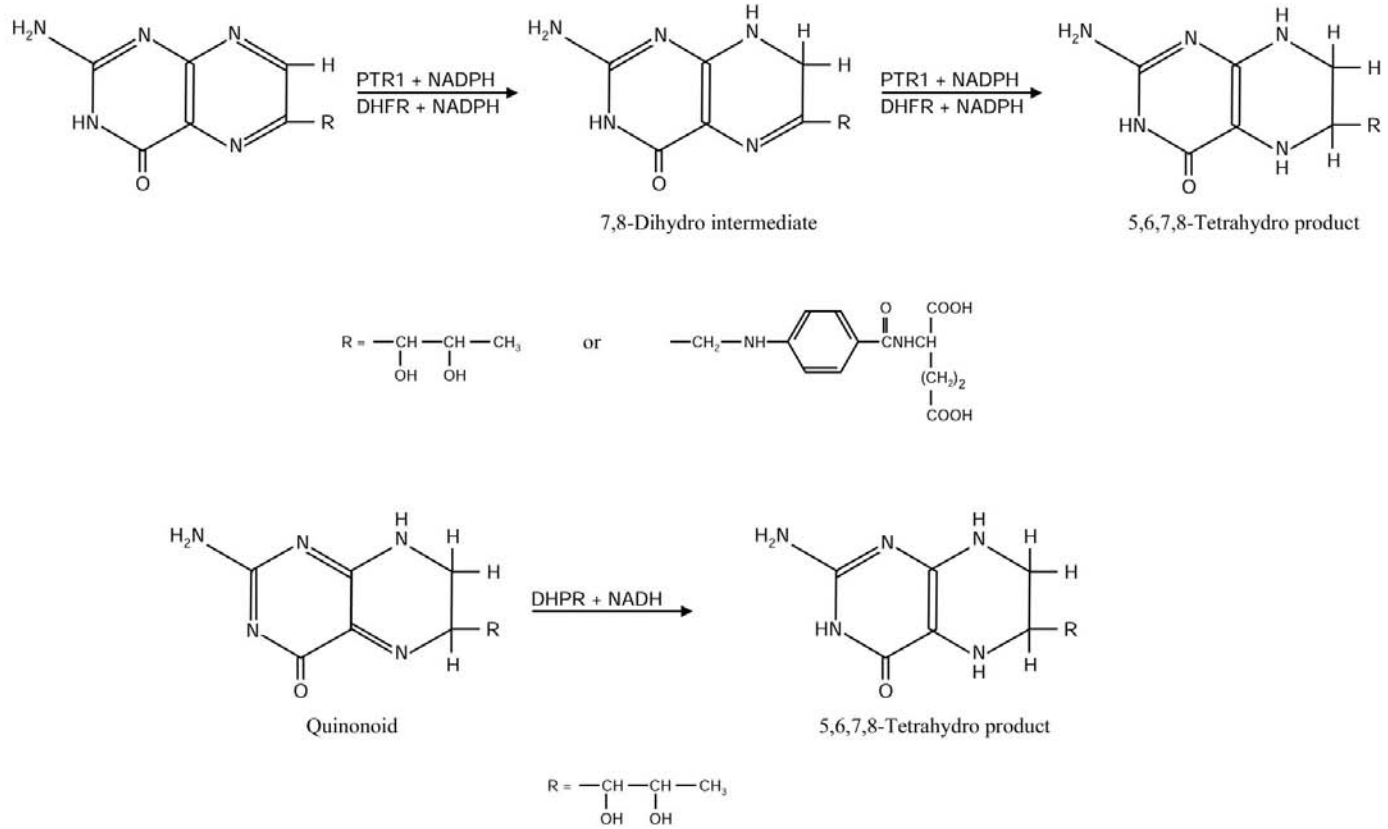

Figure 1
The catalytic pathways of PTR1, DHFR and DHPR. PTR1 and DHFR both take the fully oxidized pteridine *via* the 7,8-dihydro intermediate to the 5,6,7,8-tetrahydro product. DHPR, on the other hand, uses quinonoid dihydrobiopterin to produce tetrahydrobiopterin. PTR1 and DHFR prefer NADPH as the cofactor, whereas DHPR prefers NADH. The molecular weights of PTR1, DHFR and DHPR are 29.2, 18.1 and 25.4 kDa, respectively. The active form of PTR1 is a tetramer, that of DHFR a monomer and that of DHPR a dimer.

Table 1
Data-collection and refinement statistics.

Values in parentheses are for the highest resolution shell.

Wavelength	0.9801
Resolution (Å)	2.86
No. of measurements	215242
Unique reflections	40939
Completeness (%)	96.1
R_{sym} (%)	7.4 (39.5)
$I/\sigma(I)$	19.4 (4.4)
Refinement	
Resolution range (Å)	20–2.86
Reflections used	40720
Reflections used for R_{free}	4095
No. of residues/solvents/NADPH	1263/175/4
R/R_{free}	0.205/0.249
R.m.s deviations	
Bonds (Å)	0.007
Angles (°)	1.93

four PTR1 molecules in the asymmetric unit with a solvent content of 65%.

X-ray diffraction data were collected after flash-freezing a crystal in a nitrogen stream at 100 K. Diffraction data were collected to a resolution of 2.8 Å at BL9-2 at the Stanford Synchrotron Radiation Laboratory using an ADSC Quantum 4 CCD detector. The data were processed with the programs *DENZO* (Otwinowski & Minor, 1997) and *SCALEPACK* (Gewirth, 1993). R_{merge} was 7.4% and the completeness was 96.2%. Data-collection statistics are provided in Table 1.

2.3. Structure determination and refinement

The structure was determined using molecular-replacement techniques. Rotational and translational searches were carried out with the program *AMoRe* (Navaza, 1994), using a monomer of *L. major* PTR1 without NADPH and MTX (PDB code 1e7w) as the search model. All four molecules in the asymmetric unit forming the tetramer were located from these searches. At this stage, it became clear that the quaternary arrangement of the tetramer is the same as in the *L. major* structure and that the structure could have been solved using the tetramer of *L. major* as a search model. The starting *R* factor was 40.2%. After several cycles of simulated-annealing, positional and *B*-factor refinement using the program *CNS* (Brünger *et al.*, 1998), accompanied by rebuilding of the required regions, the *R* factor fell to 20.5% and the R_{free} fell to 24.9% for all data to 2.8 Å. Non-crystallographic symmetry restraints were not imposed during the refinements. The density of NADPH was very clear, but density of MTX was poor probably owing to a lower occupancy of the molecule. Hence, we could not precisely locate the position of the MTX molecules. In the electron-density maps, five residues at the N-terminus and a total of 21 additional residues in two solvent-exposed loop regions (Phe74–Val81 and Lys121–Lys133) were not well defined in any of the four subunits. Fig. 2 shows the electron density of NADPH and its vicinity.

3. Results and discussion

The PTR1 monomer folds into a single α/β-domain with typical short-chain reductase (SDR) topology (Jörnvall *et al.*, 1995; Varughese *et al.*, 1994). It has a central seven-stranded parallel β-sheet and six major α-helices, with three helices on each side of the sheet. Additionally, it has two minor helices, one at the carboxyl side of the β-sheet and the other at the carboxyl end of the chain. Each subunit has its own binding sites for both cofactor and inhibitor, but the functional enzyme is a tetramer in solution and in the crystal structure. In the crystal lattice, the subunits forming the tetramer are related by 222 point-group symmetry. The active site of each monomer is remote from those of other monomers in the tetramer. The active sites of momoners *A* and *D* are 25 Å apart and fall on the same side of the tetramer, while the other two sites fall on the opposite side (Fig. 3). When the four subunits assemble to form the tetramer, the C-terminus of monomer *A* comes into close proximity (4.1 Å) to that of monomer *D*. Similarly the C-termini of monomers *C* and *B* lie close to each other.

3.1. Cofactor NADPH interaction with PTR1

The catalytic center is formed from a single subunit using residues from the C-terminal regions of strands $\beta1$, $\beta2$ and $\beta3$, helix $\alpha4$ and the loops linking $\beta1$ and $\beta2$ with the N-terminal regions of $\alpha1$ and $\alpha2$. The NADPH takes up an extended conformation (Fig. 4) as in the *L. major* structure (Gourley *et al.*, 2001). This extended conformation is very similar to that of NADH in DHPR (Varughese *et al.*, 1992). The NADPH molecule binds deeply into the active site and the substrate-binding site is above the cofactor towards the mouth of the

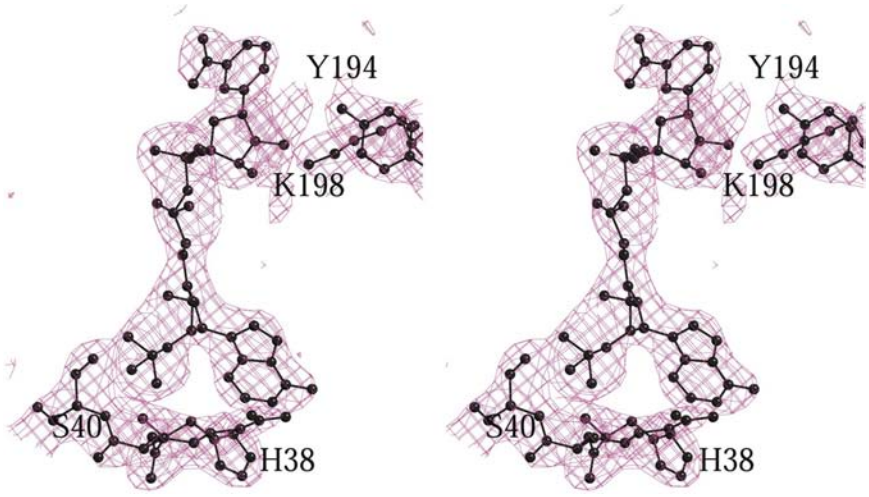

Figure 2
A stereoview of a $2F_o - F_c$ electron-density map contoured at the 1.5σ level. Electron-density contours are depicted for the cofactor NADPH, residues His38–Ser40 and the side chains of the signature residues Tyr194 and Lys198.

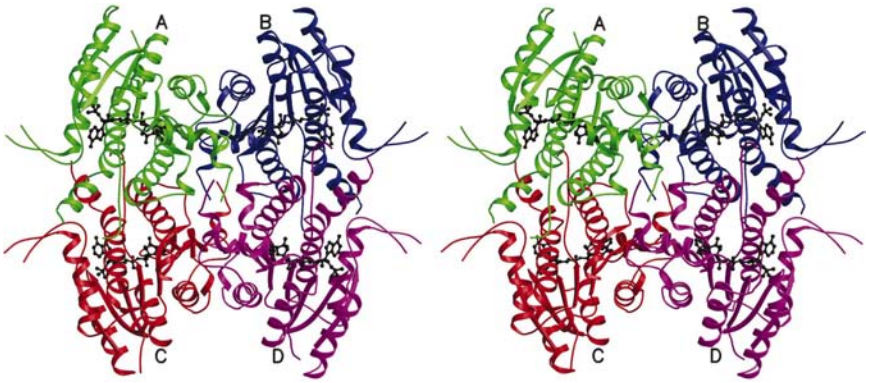

Figure 3
A stereoview of a ribbon diagram of the PTR1 tetramer. Subunits *A*, *B*, *C* and *D* are colored green, magenta, red and blue, respectively. NADPH is shown in black. The figure was produced using the program *MOLSCRIPT* (Kraulis, 1991).

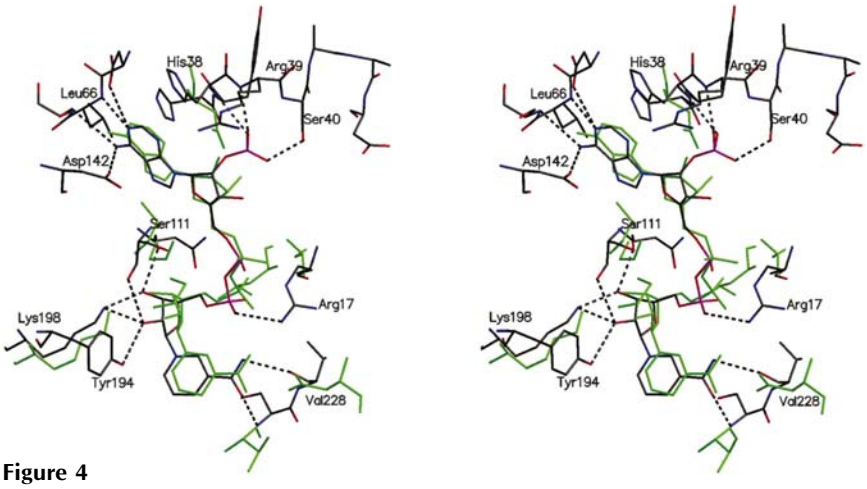

Figure 4
A stereoview showing the comparison of the NADPH binding of *L. tarentole* PTR1 with NADH binding of DHPR. DHPR and NADH are shown in green. PTR1 and NADPH are colored according to atom type.

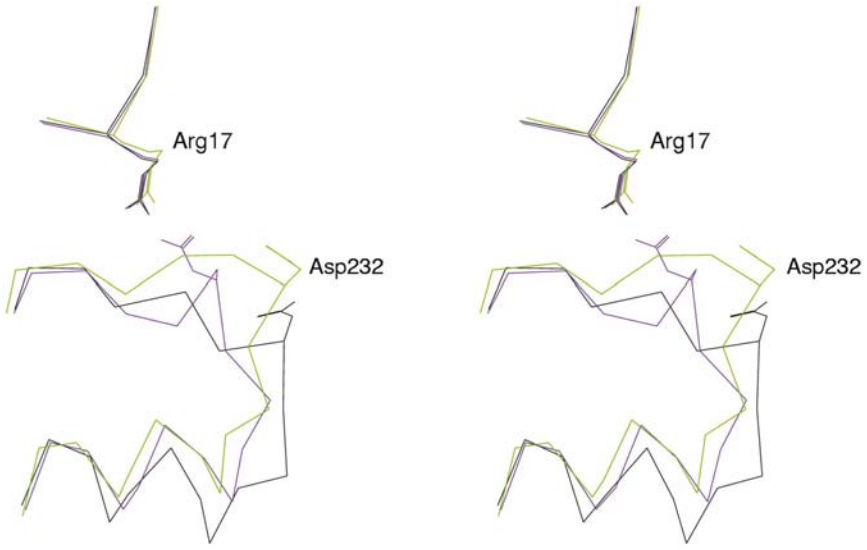

Figure 5
Comparison of loop 228–234 in PTR1 from *L. tarentole* (green), PTR1–MTX from *L. major* (purple) and PTR1–DHB from *L. major* (black). In the *L. major* MTX structure Asp232 forms a salt bridge with Arg17, while in the other two structures these residues are far apart from each other.

pocket. This provides an explanation for the sequential binding mode in which NADPH binds first (Jörnvall *et al.*, 1995). The substrate (inhibitor) can only bind effectively after the PTR1–NADPH complex has been formed. The configurations of the nicotinamide and the adenine ring are *syn* and *anti* to their respective sugar moieties. In PTR1, the consensus coenzyme-binding motif G*XXX*G*X*G (where *X* is any amino acid) is replaced by G*XXX*R*X*G. The side chain of Arg17 in this modified motif interacts with the cofactor phosphate. Generally, dinucleotide-binding proteins with a Rossmann fold have an arginine or an aspartate around the C-terminal end of strand $\beta2$, providing specificity towards NADPH or NADH. In DHPR, the carboxylates of Asp37 make two strong hydrogen bonds with the hydroxyl groups of the adenosine ribose (Varughese *et al.*, 1992). This enzyme binds NADH two orders of magnitude more strongly than NADPH (Kiefer *et al.*, 1996) and it was apparent that Asp37 was instrumental in the selectivity of the cofactor, as the negative charge of the carboxylate would repel a 2′-phosphate. To confirm this interpretation, we substituted Asp37 with an Ile and the resultant mutant enzyme had very similar 'stickiness' to both NADH and NADPH (Matthews *et al.*, 1991). Further observations showed that a basic residue in this region could form a salt bridge with the 2′-phosphate to provide specificity towards NADPH (Tanaka *et al.*, 1996). In PTR1, however, although Arg39 is in an appropriate location, the side chain of Arg39 does not interact with the phosphate. In fact, three large side chains in this vicinity (Tyr37, His38, Arg39) are oriented away from the 2′-phosphate-binding pocket to provide room for the 2′-phosphate. Interestingly, the phosphate-binding pocket is formed in a somewhat more complex way by the main-chain atoms of His38, Arg39 and Ser40, providing the enzyme with specificity towards NADPH (Fig. 4). The 2′-phosphate in *L. major* PTR1 also exhibits this peculiar binding (Gourley *et al.*, 2001).

3.2. Docking of inhibitor methotrexate (MTX)

As the density for the inhibitor MTX could not be clearly defined in the difference electron-density map, we docked MTX into the active site using the same orienta-

tion as in PTR1 from *L. major* (Gourley *et al.*, 2001). After docking, we checked for all possible interactions of MTX with the cofactor and PTR1. Most of the possible interactions were as observed in the structure of PTR1 from *L. major* (Gourley *et al.*, 2001); however, there was one major difference. In the structure of *L. major* PTR1 the loop containing residues 228–234 at the entrance of the active site makes contact with MTX, whereas this loop in the present structure is far away from the MTX-binding position. A comparison of the current structure with the *L. major* PTR1–MTX complex and the *L. major* PTR1–dihydrobiopterine complex (Fig. 5) shows a wide variation for this loop region. It therefore appears that the conformation of this loop depends on its interactions with substrate/inhibitor. Similar ligand-induced changes have been reported for many proteins, for example DHFR (Sawaya & Kraut, 1997; Cody *et al.*, 1999). Additionally, it is of interest to note that when we compared the four independent subunits in the present crystal using the program *ESCET* (Schneider, 2002), the results clearly showed that loop 228–234 is flexible and is positioned differently in various subunits.

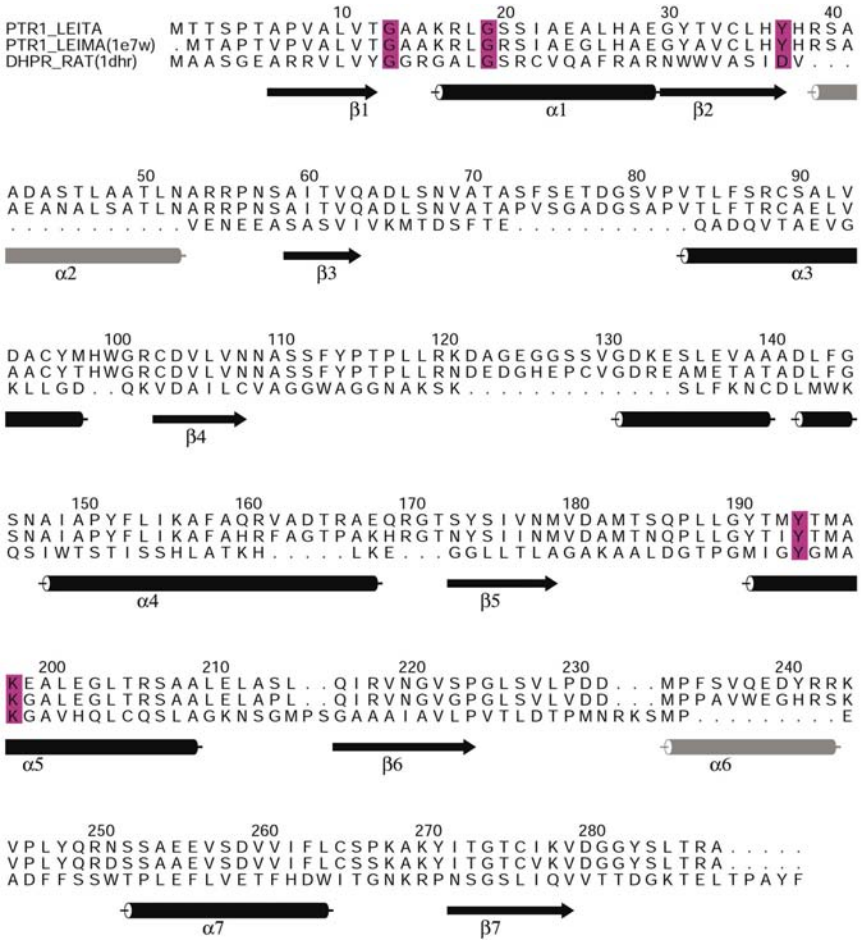

Figure 6
Sequence alignment of PTR1 from *L. tarentole*, PTR1 from *L. major* and DHPR based upon the determined three-dimensional structures. The secondary-structure elements of PTR1 are indicated with arrows for β-strands and cylinders for α-helices. Gray cylinders represent the α-helices that are absent in DHPR. The colored residues represent conservation in all SDR family members; the first three residues bind to the cofactor and the later two are the Tyr and Lys of the signature motif.

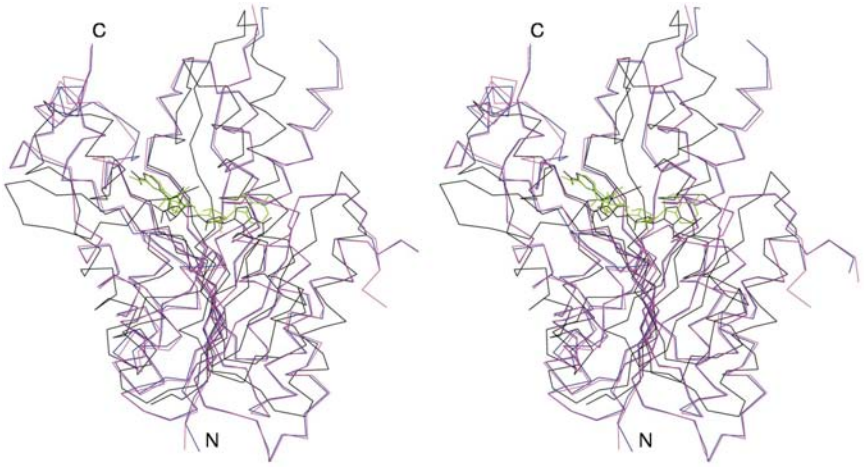

Figure 7
A stereoview of the overlay of the C^{α} trace of *L. tarentolae* PTR1 subunit (blue) with *L. major* PTR1 (magenta) and DHPR (black). This view was obtained by superimposing six β-strands of PTR1 and DHPR. NADPH is shown in green and NADH in black.

3.3. Comparisons with *L. major* PTR1 and DHPR

A sequence alignment of *L. tarentolae* PTR1, *L. major* PTR1 and DHPR is shown in Fig. 6. Several members of the SDR family are characterized by having a Ser residue located to the N-terminal side of the Tyr(Xaa)$_3$Lys motif, which is considered to form a catalytic triad along with the Tyr and Lys. It is interesting to note that the corresponding residue in PTR1 is Asp181 and in DHPR it is Ala133. The mutation of this alanine to serine in DHPR (Kiefer *et al.*, 1996) had no effect on the activity of the enzyme. In PTR1, the aspartate forms a hydrogen bond with the Tyr and can act as a proton donor, as suggested by Gourley *et al.* (2001). The superposition of the present PTR1 structure with the structures of *L. major* PTR1 (Gourley *et al.*, 2001) and rat liver dihydropteridine reductase (Varughese *et al.*, 1992) is shown in Fig. 7. The two PTR1 molecules have 79% sequence identity and the three-dimensional structures are indeed very close. On the other hand, DHPR, despite sharing the SDR fold with PTR1, differs significantly in the details of the three-dimensional structure, reflecting its somewhat differing

sequences and differing substrate and cofactor requirements. The two also differ in quaternary structure: DHPR exists as a dimer, while PTR1 is a tetramer. Mechanistically, DHPR catalyzes the reduction of quinonoid dihydrobiopterin to tetrahydrobiopterin. In contrast, PTR1 can convert biopterin to tetrahydrobiopterin in a conventional two-step reduction that does not require the higher-energy isomeric quinonoid intermediate. Additionally, PTR1 can reduce the folate molecule in a similar way. This observation suggests that the *para*-aminobenzoyl glutamate tail of the folate molecule is not important for binding at the substrate site.

The present crystal has a high solvent content of 65%, while the two *L. major* structures (Gourley *et al.*, 2001) have solvent contents of only 48% (PDB code 1e7w) and 56% (PDB code 1e92). The higher solvent content could make it easier to diffuse small-molecule inhibitors into the crystal lattice.

4. Conclusions

As *Leishmania* uses PTR1 to salvage both folates and pteridines, there is a need to develop inhibitors that block both DHFR and PTR1. Here, we present a crystal structure which may be useful for structure-based drug-design analysis. This study complements the earlier report for the PTR1 from *L. major*. The two structures together will allow regions of consistency to be determined and will also indicate flexible regions whose movements may negate specific small-molecule interactions. It becomes increasingly clear that the short-chain dehydrogenases, while preserving a common overall fold, employ sophisticated variations in the active-site regions to accomplish each specialized function.

This work was supported by the grants GM54246 and CA11778 from National Institutes of Health. MO is a Canada Research Chair Holder and a Burroughs Wellcome Fund Scholar in Molecular Parasitology. This publication is No. 15707-MEM from the Scripps Research Institute.

References

Brünger, A. T., Adams, P. D., Clore, G. M., DeLano, W. L., Gros, P., Grosse-Kunstleve, R. W., Jiang, J.-S., Kuszewski, J., Nilges, M., Pannu, N. S., Read, R. J., Rice, L. M., Simonson, T. & Warren, G. L. (1998). *Acta Cryst.* D**54**, 905–921.

Cody, V., Galitsky, N., Rak, D., Luft, J. R., Pangborn, W. & Queener, S. F. (1999). *Biochemistry*, **38**, 4303–4312.

Gewirth, D. (1993). *The DENZO Manual.* New Haven, CT, USA: Yale University and Howard Hughes Medical Institute.

Gourley, D. G., Schüttelkopf, A. W., Leonard, G. A., Luba, J., Hardy, L. W., Beverley, S. M. & Hunter, W. M. (2001). *Nature Struct. Biol.* **8**, 521–525.

Jörnvall, H., Persson, B., Krook, M., Atrian, S., Gonzàlez-Duarte, R., Jeffery, J. & Ghosh, D. (1995). *Biochemistry*, **34**, 6003–6013.

Kiefer, P. M., Varughese, K. I., Su, Y., Xuong, N. H., Chang, C. F., Gupta, P., Bray, T. & Whiteley, J. M. (1996). *J. Biol. Chem.* **271**, 3437–3444.

Kraulis, P. J. (1991). *J. Appl. Cryst.* **24**, 946–950.

Matthews, D. A., Varughese, K. I., Skinner, M., Xuong, N. H. & Hoch, J. A. (1991). *Arch. Biochem. Biophys.* **287**, 234–239.

Nare, B., Hardy, L. W. & Beverley, S. M. (1997). *J. Biol. Chem.* **272**, 13883–13891.

Nare, B., Luba, J., Hardy, L. W. & Beverley, S. M. (1997). *Parasitology*, **114**, *Suppl.*, S101–S110.

Navaza, J. (1994). *Acta Cryst.* A**50**, 157–163.

Otwinowski, Z. & Minor, W. (1997). *Methods Enzymol.* **276**, 307–326.

Ouellette, M., Drummelsmith, J., El Fadili, A., Kundig, C., Richard, D. & Roy, G. (2002). *Int. J. Parasitol.* **32**, 385–398.

Sawaya, M. R. & Kraut, J. (1997). *Biochemistry*, **36**, 586–603.

Schneider, T. R. (2002). *Acta Cryst.* D**58**, 195–208.

Tanaka, N., Nonaka, T., Nakanishi, M., Deyashiki, Y., Hara, A. & Mitsui, Y. (1996). *Structure*, **4** 33–45.

Varughese, K. I., Skinner, M. M., Whiteley, J. M., Matthews, D. A. & Xuong, N. H. (1992). *Proc. Natl Acad. Sci. USA*, **89**, 6080–6084.

Varughese, K. I., Xuong, N. H., Kiefer, P. M., Matthews, D. A. & Whiteley, J. M. (1994). *Proc. Natl Acad. Sci. USA*, **91**, 5582–5586.

Wang, J., Le Blanc, E., Chang, C. F., Papadopoulou, B., Bray, T., Whiteley, J. M., Lin, S.-X. & Ouellette, M. (1997). *Arch. Biochem. Biophys.* **342**, 197–202.